arXiv:astro-ph/9903007v1 28 Feb 1999

A TULLY-FISHER RELATION FOR S0 GALAXIES

Eyal Neistein[1], Dan Maoz[1], Hans-Walter Rix[2,3], and John L. Tonry[4]

[1] School of Physics & Astronomy and Wise Observatory, Tel-Aviv University, Tel-Aviv 69978, Israel

[2] Steward Observatory, University of Arizona, Tucson, AZ 85726

[3] Alfred P. Sloan Fellow

[4] Institute for Astronomy, University of Hawaii, 2680 Woodlawn Dr., Honolulu, HI 96822

ABSTRACT

We present an I-band Tully-Fisher relation (TFR) for 18 nearby S0 galaxies using kinematics derived from long slit spectroscopy of stellar absorption lines. Our estimates of the circular velocity, V_c, at 2-3 exponential disk scale lengths account for line-of-sight projection and for the stellar random motions through an asymmetric drift correction. Uniform and accurate distance calibration for all objects is available from surface brightness fluctuation measurements of Tonry et al. (1998). Despite the care taken in estimating both V_c and M_I, the TFR shows an *intrinsic* scatter, ~ 0.7 mag in M_I, or 0.15 in $\log_{10}V_c$. This result is surprising, as S0 galaxies appear to have both the simple kinematics of disk galaxies, and the simple stellar populations of early-type galaxies. Remarkably, in this sample of overall rotation-dominated galaxies, the central stellar velocity dispersion is a better predictor of the total I-band luminosity (through the Fundamental Plane relations) than the circular speed at several exponential scale lengths. Furthermore, the TFR zeropoint, or the mean stellar I-band luminosity at a given V_c, differs by only ~ 0.5 mag between our sample of S0s and Mathewson et al.'s (1992) sample of late-type spirals, once both data sets are brought onto a consistent distance scale. This offset is less than expected if S0s are former spiral galaxies with prematurely truncated star-formation ($\gtrsim 4$ Gyrs ago).

Subject headings: galaxies: elliptical and lenticular — galaxies: kinematics and dynamics — galaxies: photometry — galaxies: formation

1. Introduction

The Tully-Fisher relation (TFR) is a correlation between some measure of the maximal, or asymptotic, circular velocity of the disk and the integrated stellar luminosity of a galaxy. Since its discovery (Tully & Fisher 1977) much effort has been invested in studying its manifestation at various wavelengths, its dependence on different kinematic tracers, and its differences among galaxy types.

Measures of the circular velocity have been derived from either the 21cm H I line width or from optical rotation curves (e.g., Mathewson, Ford, & Buchhorn 1992; Raychaudhury et al. 1997; Giovanelli et al. 1997ab). The optical rotation curves in all these cases were derived from H II emission lines. Courteau (1997) has recently compared the TFRs based on H I widths and optical rotation curves and finds basic agreement among them. Integrated galaxy magnitudes were initially measured in the B-band and later in the I and H bands (see Aaronson et al. 1979, 1986). The slope (Aaronson & Mould 1983), the zero point, and the scatter of the TFR depend on the band (see Jacoby et al. 1992, for a summary; see also Tully et al. 1998). The lowest scatter has been found in the I band (~ 0.1 mag, Bernstein et al. 1994). Presumably, this is because the B magnitude is more influenced by dust extinction and short-lived stellar populations, while the infrared magnitude is a more robust measure of the total stellar mass of the galaxy.

While the TFR serves as a fundamental tool for measuring extragalactic distances, the physical mechanism behind its existence is also of great interest. Possible explanations for a well defined TFR are emerging (Aaronson et al. 1979; Schechter 1980; Eisenstein & Loeb 1996; Dalcanton, Spergel, & Summers 1997; Mo, Mao, & White 1998; Elizondo et al. 1998; Heavens & Jimenez 1999). Self-regulated star-formation, cosmologically-determined initial angular momentum distributions, and adiabatic baryon infall all seem to play important roles. Alternatively, Milgrom (1983; 1989) has advocated that his Modified Newtonian Dynamics (MOND), designed to explain the rotation curves of galaxies without resorting to dark matter, also naturally predicts a TFR. In the MOND picture, the instrinsic scatter in the TFR for a given galaxy population simply reflects the spread of mass-to-light ratios (M/L) in the population.

Most observational efforts have focussed on the TFR for late-type spiral galaxies, one extreme of the Hubble sequence. Rubin et al. (1985) studied the TFR for Sa, Sb and Sc galaxies, claiming a zero-point offset between Hubble types Sa and Sc that corresponds to 1.5 magnitudes in I. However, Giovanelli et al. (1997b) found an offset of only ~ 0.3 mag between these Hubble types, and Aaronson & Mould (1983), Pierce & Tully (1988), and Bernstein et al. (1994) did not find a type dependence in their TFRs. None of these authors derived a TFR for the next Hubble type, S0s, because it is difficult to measure their rotation

curves using H I or H II emission lines. Although 27% of the S0s in Roberts et al. (1991) have H I gas detected, in many of them the gas shows unusual characteristics, such as large velocity dispersions and counter-rotating components, and single-dish measurements often cannot reveal that the gas is concentrated in the inner regions or in an outer ring (e.g. Van Driel & Van Woerden 1991).

In this paper we explore an analogous relation for these earliest-type disk galaxies. S0 galaxies were classified by Hubble as a transition class between spirals and ellipticals (see van den Bergh 1997, for a recent review), and in the RSA catalog (Sandage & Tammann 1981) they comprise 11% of bright galaxies. The formation histories of S0s are not well understood and are likely to be heterogeneous. Their overabundance in cluster environments (Dressler 1980; see, e.g., Hashimoto & Oemler 1998, for an update) has led to suggestions that they are the products of disk-galaxy collisions and mergers (Schweizer 1986), or of gas stripping in later types (Gunn & Gott 1972). Numerical simulations of gas and stellar dynamics indeed suggest that the merger of two gas-rich disk galaxies of unequal mass can produce an object resembling an S0 (Hernquist & Mihos 1995; Bekki 1998a,b). In this picture, the merger induces a flow of gas to the central parts of the product galaxy, where the gas is almost completely transformed into stars during an induced central starburst. The simulated merger products resemble actual S0 galaxies in that they are much less gas-rich than their progenitors, contain a thickened disk, and exhibit little, if any, spiral structure. Observationally, this scenario is not free of problems, e.g., the absence of two distinct populations of globular clusters (old and young) in early-type galaxies (Kissler-Patig, Forbes, & Minniti 1998). As an alternative, Van den Bosch (1998) and Mao & Mo (1998) have proposed that S0s form a continuum with later types. In the context of hierarchical galaxy formation models, the bulge-to-disk ratio is a tracer of the formation redshift and/or the initial angular momentum of the dark halo in which the galaxy formed.

In their gross stuctural properties, S0s are similar to ellipticals and share the same Fundamental Plane relations (*e.g.* Jorgensen, Franx, & Kjaergard 1996). Since the central velocity dispersions of S0s and ellipticals are considerably higher than the rotation velocities of spirals of a given luminosity (which usually rise quickly to their assymptotic values), it appears that the mass-to-light ratio in the inner regions of galaxies increases when going to earlier types. The existence and parameters of a TFR for S0s could help us place them relative to ellipticals and spirals, and give a better understanding of the physical mechanism behind the TFR. From a practical viewpoint, a tight TFR for S0s could improve the distance estimate to many clusters, where S0s are the dominant population.

To our knowledge, there has been only one published effort to measure a TFR in S0 galaxies, by Dressler & Sandage (1983). They found no evidence for any actual correlation

between stellar luminosity and the observed mean stellar rotation speed. However, their rotation curves had very limited radial extent and were not corrected for projection effects nor for the stellar velocity dispersions. Furthermore, approximate (Hubble flow) distances were used, and the integrated blue magnitudes were based on photographic plates. An intrinsic TFR for S0s may have therefore been lost in the observational noise.

In this paper we attempt to measure an I-band TFR in a sample of S0 galaxies. Rotation curves are obtained from major-axis long-slit optical absorption-line spectra. In §2 we describe our sample and observations. In §3 we describe the spectroscopic and photometric reduction and analysis, present rotation curves, and derive the asymptotic circular velocities of the galaxies. In §4 we derive the TFR relation and discuss its implications. Our conclusions are summarized in §5.

2. Sample and Observations

2.1. Sample Selection

Because of the paucity of gas in S0s, the circular velocities must be estimated from stellar absorption-line kinematics, which requires fairly high signal-to-noise (S/N) ratios. We therefore first chose the brightest-possible sample of galaxies. Second, to explore or to establish any TFR we need accurate and independent distance estimates to our sample galaxies. Since the brightest S0s are nearby, Hubble distances, even when corrected for peculiar velocities using a large-scale flow model, are unreliable. We therefore chose only S0s whose distances have been measured by Tonry et al. (1998) using the surface brightness fluctuation (SBF) method (Tonry & Schneider 1988; Tonry et al. 1997; Blakeslee et al. 1998).

Specifically, our sample criteria were as follows: a) The galaxy is in the Tonry et al. (1998) sample; b) Heliocentric radial velocity < 2000 km s^{-1}; c) Declination $> -20°$; d) RSA classification S0/E, S0, SB0, S0/Sa, SB0/SBa or S0pec; e) RC3 (de Vaucouleurs et al. 1991) B magnitude < 12.6.

These criteria lead to an initial sample of nearly forty galaxies, of which we observed a sub-sample of 20, devoid of morphological peculiarities, and with inclinations $i \sim 35° - 60°$. In this inclination range both the corrections for $\sin i$ and for the line-of-sight integration through the disk (see §4) are small. Two of the galaxies, NGC 4406 and NGC 4472, were subsequently excluded from the sample because they showed little or no rotation, with their kinematics dominated by random motions. These galaxies are perhaps more suitably labeled as elliptical galaxies, which do not have a major disk component.

For three of the 18 galaxies in our final sample (NGC 936, NGC 3115, and NGC 7332) the stellar kinematics have been studied by other authors, and only photometric data were needed. For NGC 3115 we used kinematic data from Capaccioli et al. (1993) and Illingworth & Schechter (1982). A deep study of NGC 7332 by Fisher, Illingworth, & Franx (1994) provided the kinematics for this galaxy. Rotation curves for NGC 936 were taken from Kent (1987) and Kormendy (1983; 1984). Table 1 lists the objects, their parameters, and our sources of data.

2.2. Observations

Cousins I band photometry of the sample galaxies was obtained at the Wise Observatory 1m telescope using a Tektronix 1024×1024-pixel back-illuminated CCD with a scale of 0.696 ± 0.002 arcsec pixel^{-1}. For each galaxy we took $1-3$ exposures of 300 s each. Most of the images were obtained on 1995 December 29, and a few were taken on 1996 December 15 and on 1997 February 17. All nights had photometric conditions and photometric standard stars from Landolt (1992) were observed throughout each night, and used to translate counts to I-band magnitudes.

The spectroscopic observations were also obtained at the Wise Observatory 1m telescope. We used the Faint Object Spectrograph Camera (Kaspi et al. 1996) coupled to the above CCD. A $2''$-wide slit and a 600 line/mm grism, gave a dispersion of 3.68 Å pixel^{-1} in the 4000–7263 Å range, corresponding to a resolution of ~ 300 km s^{-1}. The angular sampling was 2.08 arcsec pixel^{-1}. The observations were made on 1995, October 25–26, November 29, and December 15–16, and 1996, March 14–16 and April 14–15. On each night we also obtained spectra of bright stars, mostly K-giants, to serve as templates for modeling the galaxy spectrum. Observations typically consisted of two consecutive major-axis exposures for each galaxy. Total integration times varied from 1 hr for the brightest galaxies to 4 hrs for the faintest. He-Ar lamp exposures, for wavelength calibration, and quartz lamp exposures, for flat fielding, were taken between consecutive galaxy exposures. One spectrum of NGC 5866 was obtained at Kitt Peak National Observatory (KPNO) using the 4m telescope on 1994 March 7, with the RC spectrograph, a 1200 line mm^{-1} grating and an exposure time of 30 min.

3. Data Reduction and Analysis

3.1. Photometry

The I-band images were reduced using standard IRAF[1] routines. Images were bias subtracted, and flat-field corrected using twilight sky exposures. Foreground stars were found and removed by examining each image and replacing the affected area with an interpolated two-dimensional surface, using the *Imedit* task.

In order to measure the ellipticity of each galaxy and the scale length of its disk we used the *Ellipse* task. The semi-major axis lengths of the fitted elliptical isophotes was increased in increments of 5% until the change in the intensity between two successive ellipses was negligible (except for two cases where a bright star near the galaxy prevented extracting additional isophotes). The task outputs for each ellipse the semi-major axis length, the mean isophotal intensity, the ellipticity, and the position angle. The *Elapert* task was then used to approximate each ellipse with a polygon and the counts within each polygon were measured with the *Polyphot* task. The projected disk ellipticity was taken to be the ellipticity of the last well-fitted ellipse. The disk scale length was found by χ^2 minimization, allowing the central surface-brightness, disk scale length, and sky level to vary. The parameters of the exponential disk fit and their uncertainties were used to extrapolate the counts from the last measured radius to infinity, resulting in a "total" I-band magnitude and its error. Tonry et al.'s (1998) distances to the galaxies were used to derive the absolute magnitudes, M_I. These parameters are listed in Table 1.

3.2. Spectroscopy

The long slit spectra were also reduced using standard IRAF routines. Each two-dimensional spectrum was bias subtracted. Variations in slit illumination were removed by dividing each image by an illumination image derived from a spectrum of the twilight sky. Pixel-to-pixel sensitivity variations were removed by division by a quartz lamp spectrum taken after every galaxy exposure. The quartz spectrum was first normalized by a 6th-order polynomial fit to its low frequency structure in the dispersion direction. Cosmic ray events were removed with the IRAF tasks *Ccrej*, *Cosmicrays* and *Imedit*. He-Ar arc-lamp spectra with about 40 lines were used to rectify all science frames to uniform sampling in slit position and $\log \lambda$, where λ is the wavelength, in the two cardinal directions. The resulting accuracy of the wavelength calibration is ~ 15 km s^{-1}. The sky background was removed

[1]IRAF (Image Reduction and Analysis Facility) is distributed by the National Optical Astronomy Observatories, which are operated by AURA, Inc., under cooperative agreement with the National Science Foundation.

by interpolating along the two ends of the slit, where the sky dominates. Template star spectra were reduced in the same fashion, and subsequently extracted from the frames to yield one-dimensional spectra.

The line-of-sight velocities $V_{obs}(R)$ and velocity dispersions $\sigma(R)$ as functions of the projected radius R were extracted from the galaxy spectra, following Rix & White (1992) and Rix et al. (1995). The two dimensional spectrum was first rebinned into a sequence of one-dimensional spectra of approximately constant S/N and each of these spectra was then matched by a shifted and broadened linear combination of templates, minimizing χ^2. This resulted in a kinematic profile that, at each radius, is derived from an "optimal" template.

Figure 1 (top and middle panels) shows rotation and velocity dispersion curves, $V_{obs}(R)$ and $\sigma(R)$, for the 15 galaxies we observed spectroscopically. One of the galaxies, NGC 5866, was measured both at Wise Observatory and at KPNO (see Fig. 1). Although the degradation in S/N when going to a small telescope is obvious, the agreement is good and shows that, for the present purpose the Wise Observatory spectra are of sufficient quality.

3.3. Deriving Circular Velocities from $V(R)$ and $\sigma(R)$

Determining the true circular velocity of a galaxy, defined as $V_c(R) \equiv \sqrt{R\frac{\partial \Phi_{grav}}{\partial R}}$, from stellar kinematics is somewhat model-dependent, even if rotation dominates (see, e.g., discussion by Illingworth & Schechter 1982; Binney & Tremaine 1987; Raychaudhury et al. 1997). We derive the circular velocity in several steps. When several rotation curves were available for a single galaxy (see §3.2) we computed the asymptotic velocity and velocity dispersion in each curve separately and subsequently used the means.

To obtain the mean stellar rotation velocity, V_ϕ, in the plane of the disk, we deproject the observed velocity, using the observed disk ellipticity and assuming an edge-on disk axis ratio $q_0 = 0.22$ (de Vaucouleurs et al. 1991):

$$V_\phi(R) = \frac{V_{obs}(R)}{\sin(i)} = V_{obs} \times \sqrt{\frac{1-q_0^2}{2e-e^2}} \ ,$$

where i is the inclination, e is the ellipticity, V_{obs} is the observed radial velocity, and V_ϕ is the azimuthal speed. Galaxies with ellipticities greater than 0.57 ($i > 67°$) were deemed to be edge-on, and no attempt at the above inclination correction was made.

However, in highly-inclined galaxies the line-of-sight integration through the disk will reduce the observed mean velocity relative to the actual velocity $V_\phi(R)$ at the tangent point. We constructed a simple model of an exponential disk with a vertical scale height of

$0.2R_{exp}$, to calculate $V_{obs}/V_\phi(R)$. For the edge-on case, an approximate analytic expression for $f \equiv V_{obs}/V_\phi(R)$ can be found, which is is shown in Figure 2. The same effect will lead to an overestimate of the azimuthal velocity dispersion. The two corrections for edge-on disks are:

$$V_\phi(R) = \frac{V_{obs}(R)}{f(\frac{R}{R_{exp}})} \ ,$$

$$\text{and } \sigma_\phi^2 = \sigma_{obs}^2 - \frac{1}{2}(V_\phi - V_{obs})^2 \ ,$$

$$\text{with } f(x) = \frac{\exp(-x)}{-0.5772 - \ln(x) + x - \frac{x^2}{2\times 2!} + \frac{x^3}{3\times 3!} - ...} - x,$$

where σ_ϕ is the corrected velocity dispersion, and σ_{obs} is the observed velocity dispersion. Note that our uncertainties in how close to edge-on these galaxies actually are, lead to an error of only $\Delta\log_{10}(V_\phi) \approx 0.025$, assuming random inclinations between $i = 90°$ and $i = 70°$. For inclinations less than 70°, the correction is $< 4\%$, and we neglect it.

Most importantly, however, V_c will differ from the directly observable quantities by the "asymmetric drift" correction, which accounts for the non-circular orbits of the stars, or, equivalently, their velocity dispersion. The circular velocity V_c is related to the gravitational potential Φ(R), in the galaxy plane by

$$V_c^2(R) = R\ \Big[\frac{\partial\Phi(R)}{\partial R}\Big].$$

To obtain the circular velocity (i.e. the velocity of a "cold" gas in the disk) we follow Binney & Tremaine (1987), eqn. 4-33:

$$V_c^2 = \overline{V_\phi^2} + \sigma_\phi^2 - \sigma_r^2 - \frac{R}{\rho}\frac{\partial(\rho\sigma_R^2)}{\partial R} - R\frac{\partial(\overline{V_R V_z})}{\partial z},$$

where $\rho(R) = \rho_0 \exp(-\frac{R}{R_{exp}})$ is the mass density, and the term $\overline{V_R V_z}$ is usually negligible (Binney and Tremaine, 1987). For a flat rotation curve, $\sigma_\phi^2(r)/\sigma_r^2(r) = 0.5$, which leads to

$$V_c^2 = V_\phi^2 + \sigma_\phi^2\Bigg[2\bigg(\frac{R}{R_{exp}} - \frac{\partial\ln\ \sigma_R^2}{\partial\ln\ R}\bigg) - 1\Bigg].$$

For many of the sample galaxies $\frac{\partial \ln\ \sigma_\phi^2}{\partial \ln\ R}$, and hence $\frac{\partial \ln\ \sigma_R^2}{\partial \ln\ R}$, is small, and can be neglected, yielding:

$$V_c^2 = V_\phi^2 + \sigma_\phi^2\Big(2\frac{R}{R_{exp}} - 1\Big).$$

To obtain the corrected rotation curves, we first fit an exponential function to the observed dispersion profile $\sigma_\phi(R)$. We then use the fit value of $\sigma_\phi(R)$ to apply the asymmetric drift correction to every measurement of V_ϕ for which $V_\phi/\sigma_\phi > 2.5$ (see below). The final, corrected, curves are shown in the bottom panels of Figure 1. Finally, to estimate the deprojected, asymptotic rotation speed (usually at $R \sim 3R_{exp}$), we average the last three points on either side of the corrected rotation curves in Figure 1 (bottom panels). Points with errors ≥ 100 km s^{-1} were discarded. The radius of the measured aymptotic velocity, R, was taken as the average radius of the points in the rotation curve that we used, and the uncertainty in that radius is half the distance between the inner point and the outer point that we used to obtain the final velocity.

We list all the measured and corrected velocities in Table 1. Three of the galaxies, NGC 2768, NGC 4382, and NGC 4649, have relatively large velocity dispersions even in their outer parts, such that $\sigma_\phi \gtrsim V_\phi/2.5$. Under such circumstances, the approximations and systematics involved in the asymmetric drift correction may lead to an unacceptably large error in the inferred V_c and we mark the measurements of these galaxies as uncertain in the subsequent discussion.

4. Results

With the information assembled in Table 1 we can explore the two questions posed initially: *a)* To what extent do S0s follow a TFR, i.e., how well are M_I and V_c correlated? *b)* What is the mean stellar luminosity for S0s at a given circular velocity, and how does it compare to the luminosity of later-type disk galaxies?

Figure 3 shows M_I *vs.* V_c for the sample galaxies. The errorbars in M_I include photometric errors and distance uncertainties, and the errors in V_c include propagation of all the uncertainties involved in the calculation of the final circular velocity. The data points with dotted errorbars represent the three galaxies for which the asymmetric drift corrections were uncertain due to their relatively large velocity dispersions (see above). The dashed line shows the I-band TFR for late type spiral galaxies, as derived from the Mathewson et al. (1992) data by Courteau and Rix (1998) and adjusted to the same distance scale ($H_0 = 80$ km s^{-1} Mpc^{-1}) as that implied by the SBF method for these galaxies (Tonry et

al. 1998).

To estimate the best fit and the intrinsic scatter in the TFR, we proceeded as follows (see also Rix et al. 1997.) We assumed a relation of the form

$$M_I(\log V_c) = M_I(2.3) - \alpha(\log V_c - 2.3),$$

where the fit's pivoting point is 200 km s^{-1}, i.e., $\log V_c = 2.3$. Further, we assumed that the relation has an intrinsic Gaussian scatter in M_I (at a given $\log V_c$) of σ magnitudes. For each parameter set $\left[\ M_I(2.3), \alpha, \sigma\ \right]$ this defines a model probability distribution, P_{model} in the $(M_I, \log V_c)$ plane. Each data point i, with its uncertainties in V_c and M_I, also constitutes a probability distribution in the same parameter plane, $P_i(M_I, \log V_c)$. The overall probability of a parameter set $\left[\ M_I(2.3), \alpha, \sigma\ \right]$, given the data, can be calculated as:

$$P(M_I(2.3), \alpha, \sigma) = \sum_i \int \left(P_{model} \times P_i\right)\ dM\, d\log V_c,$$

which is a measure of the overlap between the data and the model probability distributions for a given model.

It is apparent from the data (Fig. 3) that the slope is poorly determined. Therefore, we fit a relation assuming the spiral TFR slope from Mathewson et al. (1992), $\alpha = 7.5$. The best fit has a zeropoint of $M_I(2.3) = -21.36 \pm 0.15$ mag and an intrinsic scatter of $\sigma = 0.68 \pm 0.15$ mag. The thick line in Fig. 3 is this best fit relation, and the thin lines show the scatter. From the plot is is clear that the data indicate a steeper slope. Formally, $\alpha > 10.5$ (at 95% confidence), with no well-defined upper bound. Note that if we have underestimated the (dominant) velocity errors by 30%, the estimated intrinsic scatter in the relation will only decrease to ≈ 0.58 magnitudes.

Based on Figure 3, we can now answer the two question posed above:

• Despite the care taken in deriving V_c and M_I, there is a great deal of intrinsic scatter in the TFR: 0.68 ± 0.15 mag.

• At a given V_c, there is only a small (0.5 ± 0.15 mag) systematic offset in M_I, between the S0s and the Sc galaxies from Mathewson et al. This offset is much smaller than the 1.5 magnitudes (in I) between Sa's and Sc's, claimed by Rubin et al. (1985), and adds to the other evidence (e.g., Pierce & Tully 1988; Bernstein et al. 1994) that the zero point of the I-band TFR is only weakly dependent on galaxy type.

The large scatter in Fig. 3 is particularly remarkable in light of the well-behaved Fundamental Plane (FP) relation (*e.g.* Jorgensen et al. 1996, and references therein) for S0s in general, as well as for this particular set of objects. Figure 4 shows the FP for our

sample, based on values for the effective radii, R_e, as compiled in Bender, Burstein, & Faber (1992) and Fisher (1997), and central velocity dispersions, σ_0, estimated both from our data and the literature, and listed in Table 1. For comparison with the existing FP literature, we reconstructed I_{eff} from M_I and R_e, assuming a de Vaucouleur's law. The median scatter among the points is well below 0.1 in either axis.

The important difference between Figures 3 and 4 is that the FP in Figure 4 uses the *central* stellar dispersion as the kinematic parameter, while the TFR in Figure 3 involves V_c at 2–3R_{exp}, characterizing the total mass within this radius. It is clear from this comparison that, at least for this sample, the central stellar dispersion is a much better predictor of the total stellar luminosity than the circular velocity at several disk exponential radii.

We have searched for possible sources, either observational or intrinsic, for the large scatter we have found in the S0 TFR. Fisher (1997) obtained stellar rotation curves and velocity dispersion profiles for 18 S0 galaxies, 7 of which are in our sample. Although he presents his measurements only out to about one disk scale length, R_{exp}, while our rotation curves typically extend to $R/R_{exp} = 2 - 4$, a meaningful comparison can be made, since, as seen in Fig. 1, the rotation curves usually flatten out already at small radii (10 to 25 arcsec). Our measured asymptotic line-of-sight velocities agree with Fisher's at the $\sim 10\%$ level. A similar level of agreement exists between his measurements in the B-band and our measurements in I-band of the disk scale lengths and ellipticities. Velocity dispersions in his data are also generally consistent with ours, except for two cases, NGC 4382 and NGC 5866, in which he measures twice the values we obtained. NGC 4382, however, was already excluded from our analysis above because of its relatively low level of rotation, while for NGC 5866 we have both Wise Observatory data and high-quality data from KPNO, which are consistent with each other. Simien & Prugniel (1997), Bettoni & Galletta (1997), Fried & Illingworth (1994) and Seifert & Scorza (1996) have each derived rotation curves for some of the galaxies in our sample, and their results are in good agreement with ours. A mild exception is NGC 2549, for which Simien & Prugniel (1997) and Seifert & Scorza (1996) obtain a maximum velocity of 150 ± 30 km s^{-1} compared to our 113 ± 13 km s^{-1}.

While our sample has the advantage of uniform SBF distance estimation, distance errors could contribute to the TFR scatter as well. The SBF method has an r.m.s scatter of less than 0.1 mag, but there are a number of distance discrepancies which could affect a small sample like ours. Among the galaxies in our sample, Blakeslee et al. (1998) and Ciardullo et al. (1993) find differences of order of 0.3 mag between SBF-based distance modulii and distances based on planetary nebula luminosity functions for NGC 3115, NGC 4382, and NGC 1023. However, it is difficult to see how this could be a dominant source of scatter in the TFR without introducing comparable scatter in the Fundamental

Plane relation for our sample.

A second potential source of errors is in the corrections for inclination and assymetric drift we have applied to our data. These corrections are sometimes at a level of 100% (most are above 35%) and are based on noisy velocity dispersion measurements. H I observations for some of our galaxies exist, and can partially confirm the velocity corrections. Comparisons of H I velocities and corrected stellar velocities are not straightforward, since the gas component in S0s may sometimes be concentrated only in the inner parts or in an outer ring, as a relic from a past accretion event. Furthermore, there are different measures of 21 cm linewidth (e.g., at 50% or 20% of the peak). Nevertheless, from Roberts et al. (1991), Huchtmeier et al. (1995), and Wardle & Knapp (1986) we obtained H I velocities for five galaxies in our sample, and find excellent agreement with our corrected stellar velocities in four cases, the exception being NGC 1052, where there is a $\sim 2\sigma$ discrepancy between the inclination-corrected H I width of Roberts et al. (1991), 288 km s^{-1}, and our final circular velocity of 190 ± 39 km s^{-1}. As an alternative method of calculating the assymetric drift correction, we attempted, instead of the procedure decribed above, to apply the correction directly to the outermost measurements of the velocities and dispersions, after averaging the outer three points. However, this had the effect of increasing the scatter in the TFR. This is a consequence of the large R/R_{exp} values making the dispersion term in the assymetric drift correction, $\sigma_\phi^2\left(2\frac{R}{R_{exp}} - 1\right)$, dominant compared to V_ϕ^2. Modifications in the choice of R, or correcting σ_ϕ for inclination had little effect on the TFR scatter.

Next, we searched for intrinsic sources of TFR scatter, arising from a possible dependence on additional parameters. We have checked for correlations among the residuals in the best-fitting TFR relation and a variety of parameters. We found no dependence of TFR residuals on disk ellipticity, as was found, e.g., in the late-type-galaxy TFR of Bernstein et al. (1994) and interpreted as the effect of extinction by dust. The ratio $\frac{V_\phi}{\sigma_0}$ can serve as a kinematic indicator of rotational vs. dispersive support in a given galaxy, and correlation of the TFR residuals with it could indicate, e.g., that those galaxies with the least rotation (and the largest assymetric drift corrections) are those contributing most to the scatter. However, we found no significant correlation between the TFR residuals and this ratio. Similarly the residuals are not correlated with $\frac{R_{exp}}{R_e}$, a photometric measure of disk vs. bulge dominance. We found that the parameter $x = \frac{V_\phi}{\sigma_0} - \frac{R_{exp}}{R_e}$ is marginally correlated with the TFR residuals, at a significance level of 93%. Although the physical significance of x is unclear, applying this correction reduces the intrinsic TFR scatter by ~ 0.2 mag.

In view of these tests, we conclude that the large intrinsic TFR scatter of 0.7 mag that we find for S0s is most likely not the result of errors in observation and analysis.

Likewise, we have not found additional parameters that significantly lower the scatter. For comparison, the TFR in late type spirals usually has an intrinsic r.m.s scatter of $\sigma_{in} \sim 0.25$ mag (e.g. Giovanelli et al. 1997b), although a smaller scatter can occur in homogeneous, well-defined samples; Bernstein et al. (1994) found an r.m.s. scatter of 0.23 mag, which, after correction for extinction based on ellipticities reduced to 0.1 mag.

From the physical viewpoint, our result is in conflict with the idea that most S0s were disk galaxies – on their way to become present day spirals – whose star-forming career was cut short by some mechanism, e.g. tidal stripping in a dense environment (Gunn & Gott 1972). In that case, we would expect the S0s to have faded significantly at constant V_c, exhibiting a larger TFR zeropoint offset. Specifically, if S0s had had similar star formation histories to Sc's (e.g., Kennicutt et al. 1994) until a truncation, say, $\gtrsim 4$ Gyrs ago, we would expect an offset of $\gtrsim 0.9$ magnitudes in I due to the fading of the stellar population, based on Charlot & Bruzual (1991) models.

Similarly, the absence of a tight S0 TFR argues against a physical continuity of S0s with later-type spirals, as suggested in the context of hierarchical structure formation models (Van den Bosch 1998; Mao & Mo 1998). Alternatively, S0s may be more closely related to ellipticals. Both may be the relics of non-cataclysmic mergers (Schweizer 1986). For individual sample members, (*e.g.* NGC 4649, NGC 4406, NGC 4472) this may be apparent from their individual structure, but the present evidence is pointing towards this being true for a good fraction of the morphological class. Qualitatively, the spread among S0s in time elapsed since the merger and its ensuing gas-depleting starburst would produce the TFR scatter, while, on average, the larger concentration of stars may compensate for the fading of the stellar population, and give a mean luminosity comparable to that of late-type galaxies, for a given halo mass. A quantitative examination of the TFR resulting in this scenario is, however, needed.

5. Conclusions

We have constructed a TFR for nearby S0 galaxies, deriving corrected circular velocities from stellar velocities, and using high-quality distance estimates (Tonry et al. 1998) based on surface brightness fluctuations. Despite the care taken, the relation between M_I and V_c exhibits ~ 0.7 magnitudes of scatter. As an illustration, NGC 2787 and NGC 4753 both have similar circular velocities of 230 km s^{-1}, but their luminosities differ by over 3 mag. The reason for this large scatter is not clear. Perhaps it indicates that the S0 morphological class truly represents a "mixed bag", with a wide range of galaxy formation channels feeding into it. The central stellar velocity dispersion is a much better predictor of the total

stellar luminosity than V_c at several exponential radii.

Similarly, the fact that on average S0's and Sc's of the same V_c have such similar luminosities is a puzzle. S0s have older, and hence dimmer, stellar populations, which should lead to a TFR zero-point offset. The absence of such an offset could be explained if S0s have a considerably higher fraction of their total mass in stars than Sc's. This perhaps would be expected in the merger-formation scenario if, in fact, such events are very efficient at converting the available gas into stars.

Observationally, it is desirable to reconfirm our result on a larger sample with higher S/N measurements at larger radii, where presumably the kinematic corrections will be smaller. An independent test, which is insensitive to errors in the distance estimate, is to measure the TFR for S0s in a galaxy cluster. Analysis of such a measurement for the Coma cluster is underway (Hinz, Rix, & Bernstein 1999).

We thank Rachel Somerville for useful discussions, and the referee, Brent Tully, for helpful comments. This work was supported by the US-Israel Binational Science Foundation Grant 94-00300, and by the Alfred P. Sloan Foundation (HWR).

REFERENCES

Aaronson, M., Huchra, J. & Mould, J. 1979, ApJ, 229, 1

Aaronson, M. & Mould, J. 1983, ApJ, 265, 1

Aaronson, M., Bothun, G., Mould, J., Huchra, J., Schommer, R.A. & Cornell, M.E. 1986, ApJ, 302, 536

Bekki, K. 1998a, ApJ, in press, astro-ph/9804220

Bekki, K. 1998b, ApJL, in press, astro-ph/9806106

Bender, R., Burstein, D., & Faber, S.M. 1992, ApJ, 399, 462

Bernstein, G.M., Guhathakurta, P., Raychaudhury, S., Giovanelli, R., Haynes, M.P., Herter, T., & Vogt, N.P. 1994, AJ, 107, 1962

Bertola, F., Buson, L.M. & Zeilinger, W.W. 1992, ApJ, 401, L79

Bettoni, D., & Galletta, G. 1997, A&AS, 124, 61

Blakeslee, J.P., Ajhar, E.A., & Tonry, J.L. 1998, in *Post-Hipparcos Cosmic Candles*, A. Heck & F. Caputo (eds), (Dordrecht: Kluwer), astro-ph/9807124.

Capaccioli, M., Cappellaro, E., Held, E.V, & Vietri, M. 1993 , A&A, 274, 69

Capaccioli, M. & Longo, G. 1994, A&ARv, 5, 293

Charlot, S. & Bruzual, G., 1991, ApJ, 367, 126.

Ciardullo, R., Jacoby, G.H., & Tonry, J.L. 1993, ApJ, 419, 479

Courteau, S., & Rix, H.-W. 1998, ApJ, *submitted*.

Dalcanton, J.J., Spergel, D.N., & Summers, F.J. 1997, ApJ, 482, 659

de Vaucouleurs, G., de Vaucouleurs, A., Corwin, H. G., Buta, R. J., Paturel, G., & Fouqué, P. 1991, Third Reference Catalog of Bright Galaxies (New York: Springer) (RC3)

Dressler, A. 1980, ApJ, 236, 351

Dressler, A. 1987, ApJ, 317, 1

Dressler, A., & Sandage, A. 1983, ApJ, 265, 664

Eisenstein, D.J. & Loeb, A. 1996, ApJ, 475, 421

Elizondo, D., Yepes, G., Kates, R, Müller, V., & Klypin, A. 1998, ApJ, submitted, astro-ph/9808287

Elson, R.A.W. 1997, MNRAS, 286, 771

Faber, S.M., & Jackson, R.E. 1976, ApJ, 204, 668

Fisher, D., Illingworth, G., & Franx, M. 1994, AJ, 107, 160

Fisher, D., Illingworth, G., & Franx, M. 1995, ApJ, 438, 539

Fisher, D. 1997, AJ, 113, 950

Fried, J.W., & Illingworth, G.D. 1994, AJ, 107, 992

Giovanelli, R., et al. 1997a, AJ, 113, 22

Giovanelli, R., et al. 1997b, AJ, 113, 53

Gunn, J.E., & Gott, J.R. 1972, 176, 1

Hashimoto, Y., & Oemler, A. 1998, ApJ, in press, astro-ph/9807275

Heavens, A.F., & Jimenez, R. 1999, MNRAS, in press

Hernquist, L., & Mihos, J.C. 1995, 448, 41

Hinz, P., Rix, H.-W., & Bernstein, G.M. 1999, in preparation

Huchtmeier, W.K., Sage, L.J., Henkel, C. 1995, A&A, 300, 675

Illingworth, G.D., & Schechter, P.L. 1982, ApJ, 256, 481

Jacoby, G.H., Ciardullo, R., & Ford, H.C. 1990, ApJ, 356, 332

Jacoby, G.H., et al. 1992, PASP, 104, 599

Jedrzejewski, R.I. 1987, MNRAS, 226,747

Jorgensen, I., Franx, M., & Kjaergaard, P. 1996, MNRAS, 280, 167

Kaspi, S., Ibbetson, P.A., Mashal, E., & Brosch, N. 1996, Wise Obs. Tech. Rep., No 6

Kent, S.M. 1987, AJ, 93, 1062

Kennicutt, R., Tamblyn, P. & Congdon, C., 1994, ApJ, 435, 22.

Kissler-Patig, M., Forbes, D.A., & Minniti, D. 1998, MNRAS, in press, astro-ph/9804261

Kormendy, J. 1983, ApJ, 275, 529

Kormendy, J. 1984, ApJ, 286, 132

Kuijken, K., Fisher, D., & Merrifield, M.R. 1996, MNRAS, 283, 543

Landolt, A.U. 1992, AJ, 104, 340

van der Marel, R.P., & Franx, M. 1993, ApJ, 407, 525

Mao, S., & Mo, H.J. 1998, MNRAS, submitted

Mathewson, D.S., Ford, V.L., & Buchhorn, M. 1992, ApJS, 81, 413

Milgrom, M. 1983, ApJ, 270, 365

Milgrom, M. 1989, ApJ, 338, 121

Persic, & M., Salucci, P. 1995 in *Astroph. Lett. & Comm.:Proceedings of the 3rd Italian Cosmology Meeting* (astro-ph/9503051)

Pierce, R. & Tully, R.B. 1988, ApJ 330, 579

Raychaudhury, S., Von Braun, K., Bernstein, G.M., & Guhathakurta, P. 1997, AJ, 113, 2046

Rix, H.W., & White, S.D.M. 1992, MNRAS, 254, 389

Rix, H.W., Kennicutt, R.C.J., Braun, R., & Walterbros, R.A.M. 1995, ApJ, 438, 155

Rix, H.-W., Guhathakurta, P., Colless, M., & Ing. K. 1997, MNRAS, 285, 779

Roberts, M.S., Hogg, D.E., Bregman, J.N., Forman, W.R., & Jones, C. 1991, ApJS, 75, 751

Rubin, V.C., Burstein, D., Ford, W.K., & Thonnard, N. 1985, ApJ, 289, 81

Sandage, A., & Tammann, G. 1981, A Revised Shapley-Ames Catalog of Bright Galaxies (Washington D.C.: Carnegie Institution Pub. 638) (RSA)

Schechter, P. 1980, AJ, 85, 801

Schweizer, F. 1986, Science, 231, 193

Seifert, W., & Scorza, C. 1996, A&A, 310, 75

Simien, F., & Prugniel, P. 1997, A&AS, 126, 519

Steiman-Cameron, T.Y., Kormendy, J., & Durisen, R.H. 1992, ApJ, 104, 1339

Tonry, J.L. & Schneider, D.P. 1988, AJ, 96, 807

Tonry, J.L., Blakeslee, J.P., Ajhar, E.A., & Dressler, A. 1997, ApJ, 475, 339

Tonry, J.L., Ajhar, E.A., Blakeslee, J.P., & Dressler, A. 1998, in preparation

Tully, R.B, & Fisher, J.R. 1977, A&A, 54, 661

Tully, R.B., Pierce, M.J., Huang, J.-S., Saunders, W., Verheijen, M.A.W., & Witchalls, P.L. 1998, AJ, 115, 2264

Van den Bergh, S. 1997, AJ, 113, 2054

Van den Bosch, F.C. 1998, ApJ, submitted, astro-ph/9805113

Van Driel, W., & Van Woerden, H. 1991, A&A, 243, 71

Wardle, M., & Knapp, G.R. 1986, AJ, 91, 23

This preprint was prepared with the AAS LaTeX macros v4.0.

TABLE 1. Galaxy Parameters

NGC (1)	V_h (2)	Class. (3)	B (4)	S (5)	ellip. (6)	i (7)	R_{exp} (8)	I (9)	R (10)	V_{obs} (11)	V_ϕ (12)	V_c (13)	σ_ϕ (14)	D (15)	M_I (16)	σ_0 (17)	R (18)
584	1875	S0(3.5)	11.2	1	0.34± 0.02	50	8.5± 1.4	9.86± 0.05	47.8± 16.6	150± 23	195± 30	251 ±50	75± 10	31.45± 0.10	-21.59± 0.11	225	24
936	1404	SB0/SBa	11.2	3	0.25± 0.25	42	15.7± 1.4	10.23± 0.06	60.3± 10.4	179± 14	265±115	334 ±95	79± 15	31.82± 0.15	-21.59± 0.16	193	25
1023	661	SB0(5)	10.4	1	0.61± 0.03	70	61.1± 18.2	7.72± 0.15	79.0± 37.4	192± 9	204± 9	250 ±17	59± 20	30.24± 0.16	-22.52± 0.22	213	38
1052	1471	E3/S0	11.5	1	0.27± 0.05	44	17.3± 2.1	9.30± 0.05	41.6± 20.8	99± 13	141± 21	190 ±39	52± 26	31.22± 0.22	-21.92± 0.23	204	37
2549	1082	S0(7)	12.2	1	0.60± 0.02	69	20.2± 2.1	9.90± 0.04	27.0± 16.6	113± 13	145± 18	195 ±32	73± 16	30.35± 0.23	-20.45± 0.24	155	21
2768	1408	S0(6)	11.0	1	0.55± 0.03	65	44.8± 8.4	8.73± 0.08	62.4± 41.6	107± 16	117± 17	250 ±40	73± 20	31.86± 0.17	-23.13± 0.18	193	61
2787	664	SB0/a	11.7	1	0.41± 0.02	55	30.4± 2.8	9.06± 0.04	47.8± 35.4	171± 14	207± 17	233 ±33	73± 20	28.99± 0.33	-19.93± 0.33	205	..
3115	655	S0(7)	10.0	4	0.58± 0.07	67	41.0± 4.9	7.68± 0.05	99.8± 79.0	262± 9	305± 19	369 ±61	105± 10	29.82± 0.11	-22.14± 0.12	220	36
3384	770	SB0(5)	10.7	1	0.46± 0.02	59	55.5± 11.9	8.15± 0.09	52.0± 31.2	170± 17	197± 20	245 ±30	87± 30	30.11± 0.15	-21.96± 0.18	140	29
3412	861	SB0(5)	11.5	1	0.42± 0.02	56	30.9± 4.9	9.07± 0.06	47.8± 27.0	91± 9	109± 10	200 ±34	52± 17	30.20± 0.12	-21.13± 0.13	105	22
3489	659	S0/Sa	11.1	1	0.45± 0.04	58	19.4± 1.4	9.09± 0.04	37.4± 27.0	105± 20	123± 23	180 ±50	78± 28	30.30± 0.15	-21.21± 0.15	125	18
4251	1014	S0(8)	11.6	1	0.36± 0.10	51	22.6± 2.8	9.41± 0.05	72.8± 31.2	139± 16	161± 19	215 ±40	61± 18	31.37± 0.18	-21.96± 0.19	120	20
4382	773	S0(3)pec	10.1	1	0.29± 0.05	45	50.3± 13.3	7.73± 0.12	72.8± 31.2	84± 13	116± 19	300 ±40	86± 20	31.45± 0.14	-23.72± 0.18	190	23
4649	1259	S0(2)	9.8	1	0.20± 0.02	37	29.6± 5.6	7.89± 0.07	62.4± 20.8	109± 9	177± 16	378 ±99	186± 59	30.97± 0.14	-23.08± 0.16	350	74
4753	1288	S0pec	10.9	1	0.42± 0.04	56	34.8± 2.8	8.61± 0.04	39.5± 25.0	133± 7	159± 10	233 ±19	60± 17	31.69± 0.15	-23.08± 0.16	220	..
4754	1461	SB0(5)	11.4	1	0.46± 0.04	59	61.3± 19.6	8.68± 0.14	47.8± 35.4	159± 16	185± 19	270 ±41	52± 20	31.00± 0.14	-22.32± 0.20	171	13
5866	692	S0(8)	10.9	2	0.57± 0.01	67	21.0± 3.5	8.88± 0.07	72.8± 20.8	159± 7	185± 9	265 ±21	89± 14	30.82± 0.10	-21.94± 0.12	140	33
7332	1211	S0(8)	11.7	5	0.70± 0.01	76	19.7± 1.4	9.77± 0.04	33.3± 8.3	137± 7	176± 10	206 ±16	75± 9	31.72± 0.17	-21.95± 0.18	136	11

Notes to Table 1.

All velocities in km s^{-1}; all lengths in arcseconds. ± columns denote 1σ uncertainties. Column header explanations: (1) NGC number; (2) Heliocentric velocity, from deVaucouleurs et al. (1991); Classification, from Sandage & Tamann (1981); (4) B magnitude, from deVaucouleurs et al. (1991); (5) Source of spectroscopic data: 1=Wise Observatory, 2=KPNO, 3=Kent (1987), 4=Capacc et al. (1993), 5=Fisher et al. (1994); (6) Disk ellipticity in the I band; (7) Inclination, in degrees; (8) Exponential disk scale length; (9) Integrated I magnitude; (10) Radius of outermost veloc measurement; (11) Observed velocity at R (12) Rotation velocity at R, after correction for inclination or line-of-sight integration; (13) Circular velocity, after correction for asymmetric drift; (Observed velocity dispersion at R; (15) Distance modulus; (16) Absolute I magnitude; (17) Central velocity dispersion; (18) Effective radius, from literature.

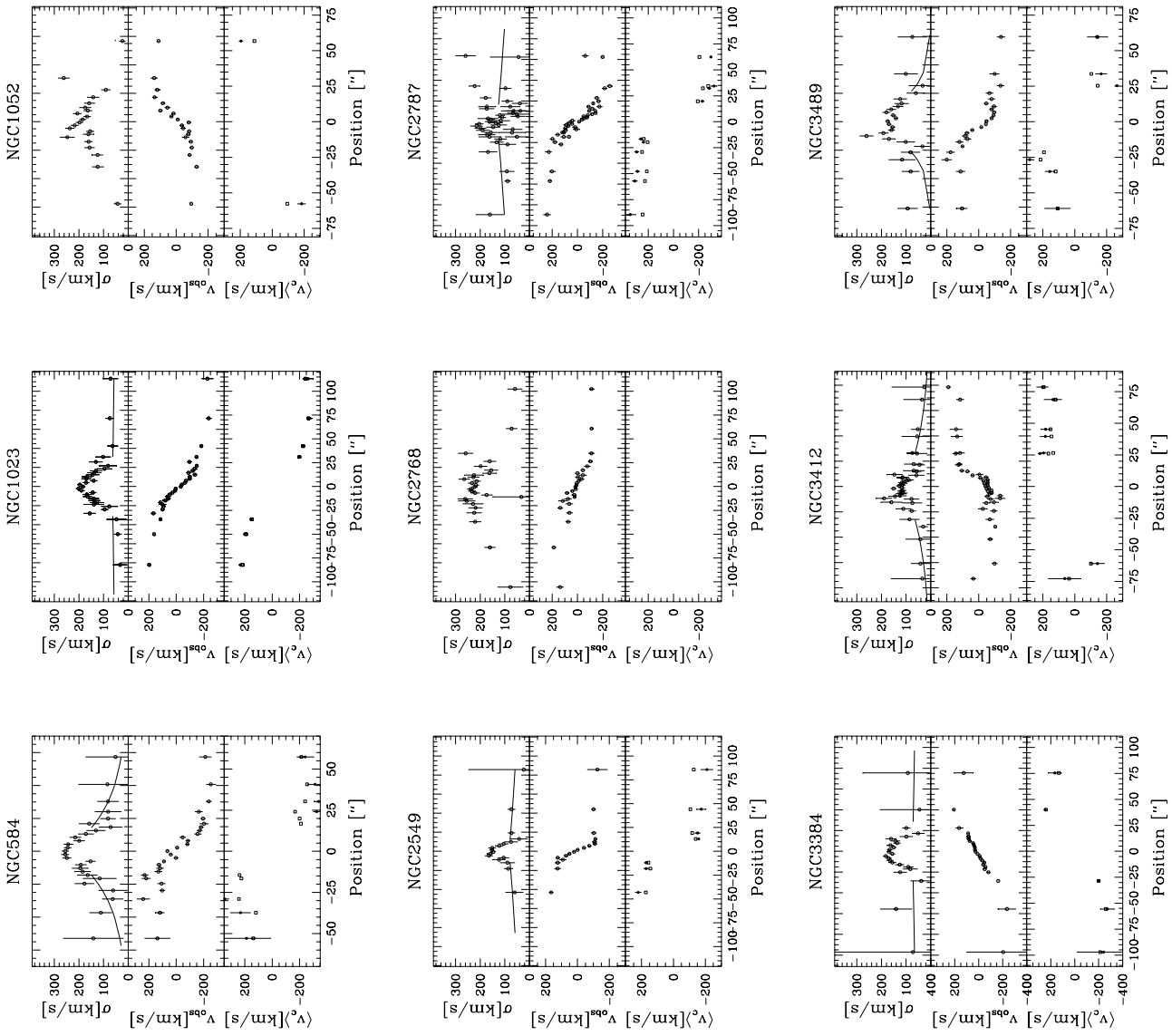

Fig. 1.— Rotation and velocity dispersion curves, $V(R)$ and $\sigma(R)$, for the 15 galaxies observed spectroscopically. Top panels show the observed velocity dispersion profiles, $\sigma_\phi(R)$. Middle panels show the observed rotation curves $V_{obs}(R)$. Bottom panels show the observed rotation curves (empty symbols) and the circular velocity (filled symbols), $V_c(R)$, after correction for inclination or integration along the line of sight and asymmetric drift correction.

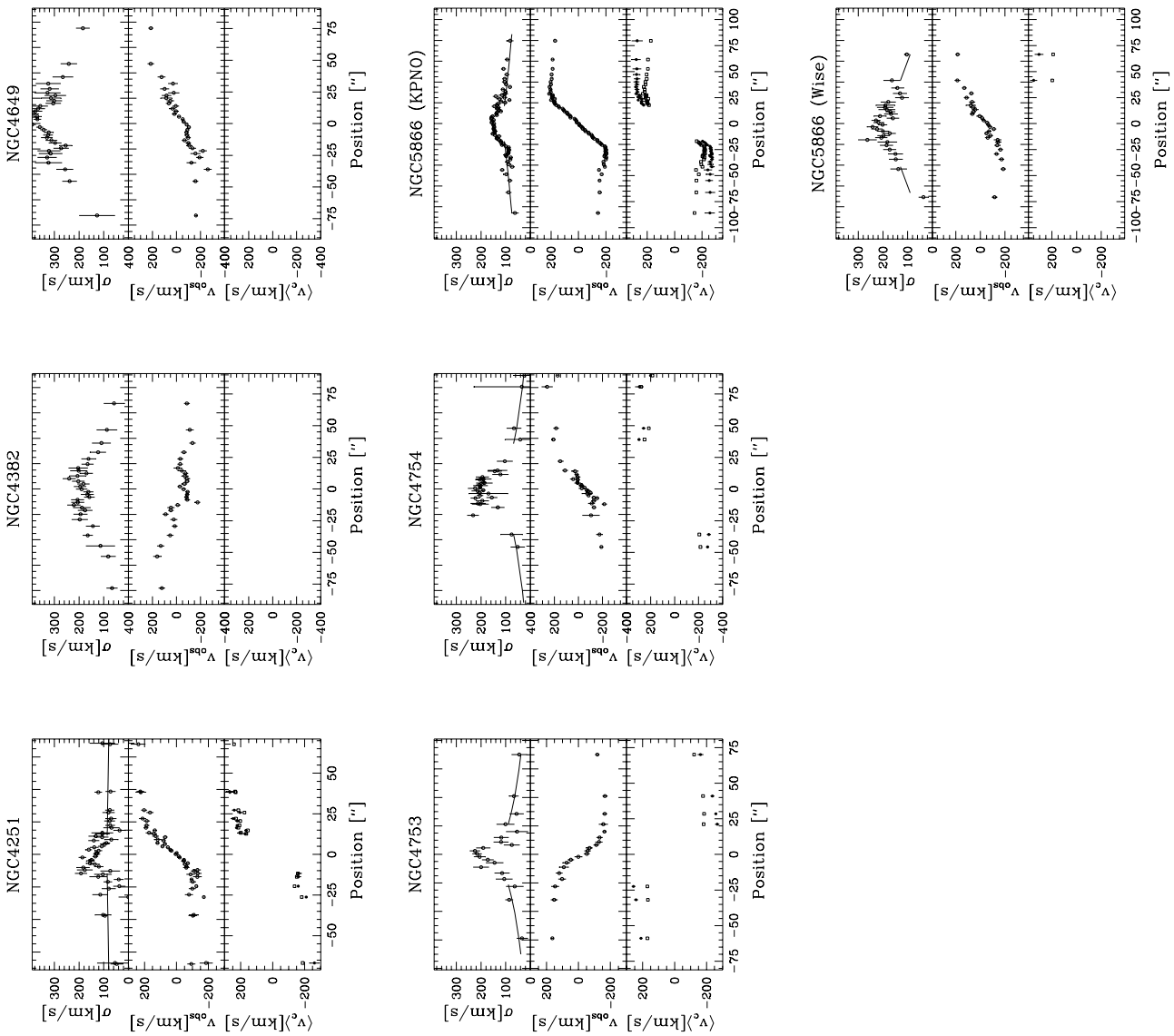
NGC4649
NGC5866 (KPNO)
NGC5866 (Wise)
NGC4382
NGC4754
NGC4251
NGC4753
σ[km/s]
⟨v_c⟩[km/s] v_obs[km/s]
Position ["]

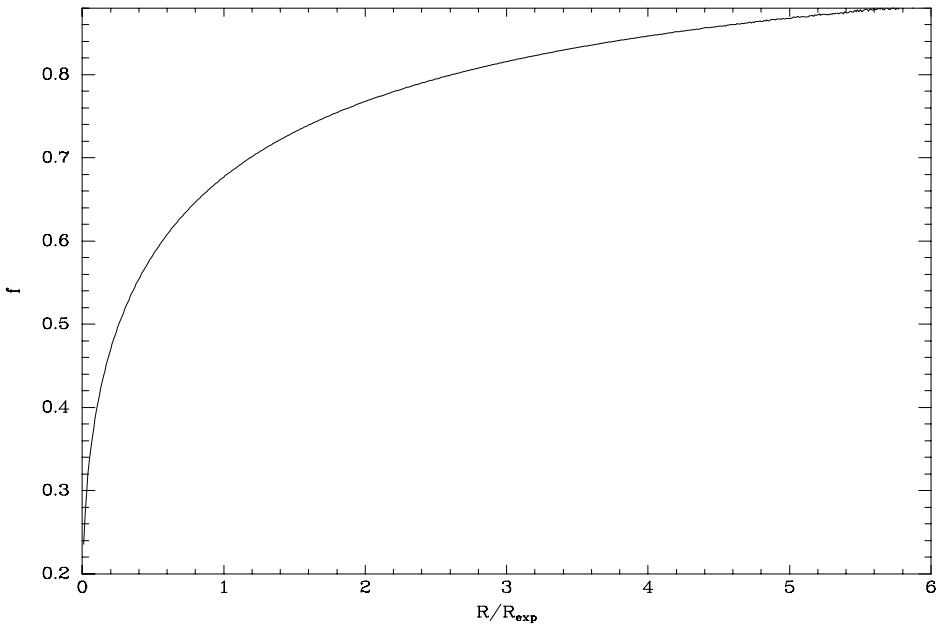

Fig. 2.— The correction function $f(R/R_{\rm exp})$, which we apply to the observed velocity of nearly edge-on galaxies to account for integration along the line of sight.

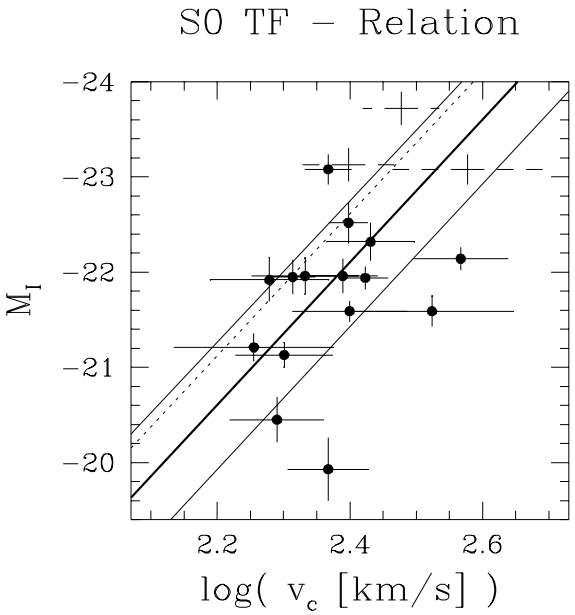

Fig. 3.— M_I *vs.* V_c for our sample galaxies. The data with dotted errorbars indicate the objects which have relatively large velocity dispersions even in their outer parts, leading to asymmetric drift corrections $\geq 25\%$. The dashed line shows the I-band TFR for late-type spiral galaxies, as derived from the Mathewson et al. (1992) data by Courteau and Rix (1998) and adjusted to the same distance scale ($H_0 = 80$ km s^{-1} Mpc^{-1}) as that implied by the SBF method for these galaxies (Tonry et al. 1998). The thick solid line shows the best fit relation, when constrained to have the same slope as the late-types, and the thin lines mark the intrsinsic scatter.

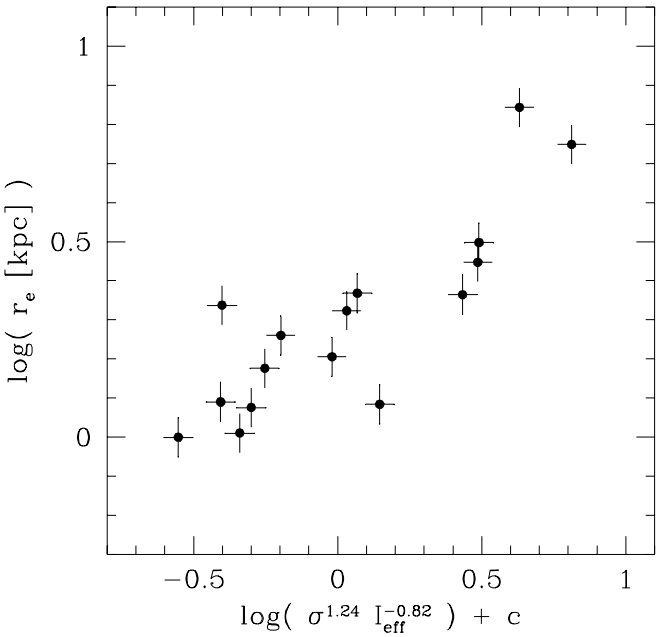

Fig. 4.— Fundamental Plane relation for our sample, based on values for the effective radii, R_e, and and the central velocity dispersions, σ_0, taken both from our data and from the literature. The median scatter among the points is well below 0.1 in either axis.